ELSEVIER

Nuclear Instruments and Methods in Physics Research A 472 (2001) 533–540

NUCLEAR INSTRUMENTS & METHODS IN PHYSICS RESEARCH Section A

www.elsevier.com/locate/nima

Towards accurate simulation of fringe field effects

M. Berz*, B. Erdélyi, K. Makino

Department of Physics and Astronomy, National Superconducting Cyclotron Laboratory, Michigan State University, East Lansing, MI 48824, USA

Abstract

In this paper, we study various fringe field effects. Previously, we showed the large impact that fringe fields can have on certain lattice scenarios of the proposed Neutrino Factory. Besides the linear design of the lattice, the effects depend strongly on the details of the field fall off. Various scenarios are compared. Furthermore, in the absence of detailed information, we study the effects for the LHC, a case where the fringe fields are known, and try to draw some conclusions for Neutrino Factory lattices. © 2001 Elsevier Science B.V. All rights reserved.

PACS: 41.85.−p; 05.45.−a

Keywords: Fringe fields; Normal form; Muon accelerators; LHC

1. Introduction

While the nonlinear effects induced by fringe fields have been studied in the spectrograph community for a long time, their careful treatment in accelerator facilities design is just beginning, after their presence was shown to have consequences on the nonlinear motion in certain scenarios. In Ref. [1], we presented a detailed analysis of generic fringe field effects. We showed that in general both the fringe fields' length and details of their fall-off shape does influence the linear and nonlinear single particle dynamics.

The consequences of the fringe fields are particularly important for small rings of large acceptance, and for beams of large emittance. Such facilities include the proposed Neutrino Factory [2], the SNS accumulator ring [3], and others. We showed that generic fringe fields, if not accounted for, have a significant impact on the dynamic aperture of a lattice of the Neutrino Factory [4]; for an example, see Fig. 1.

The details of the fringe fields induce considerable differences in some nonlinear dynamics indicators [1]. We applied six different fringe field shapes to all elements of the above mentioned Neutrino Factory. We used some quasi-realistic fringe field shapes (measurements fitted to Enge functions), and different magnet apertures. For example, merely changing the shape of the fringe field fall off leads to the two rather different shapes of the tracking pictures shown in Fig. 2.

Table 1 represents the results of the computation of some of the amplitude dependent tune shifts in the horizontal plane for many fringe field shapes and one aperture. For more details, we refer the reader to Ref. [1].

All these facts point out the importance of the fringe fields in general, and the relevance of

*Corresponding author.
E-mail address: berz@msu.edu (M. Berz).

PII: S0168-9002(01)01304-3

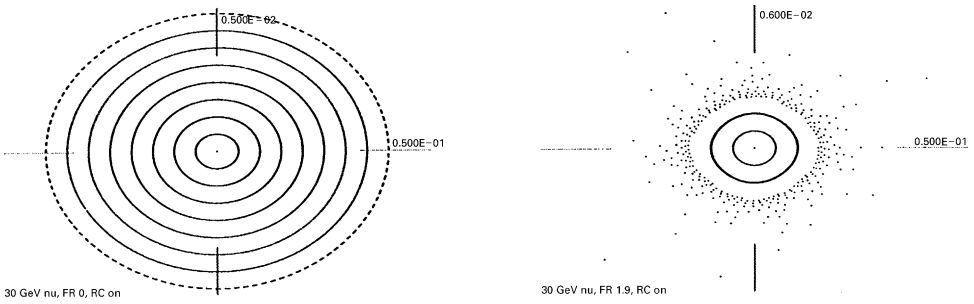

Fig. 1. Neutrino Factory tracking without fringe fields, and with generic fringe fields.

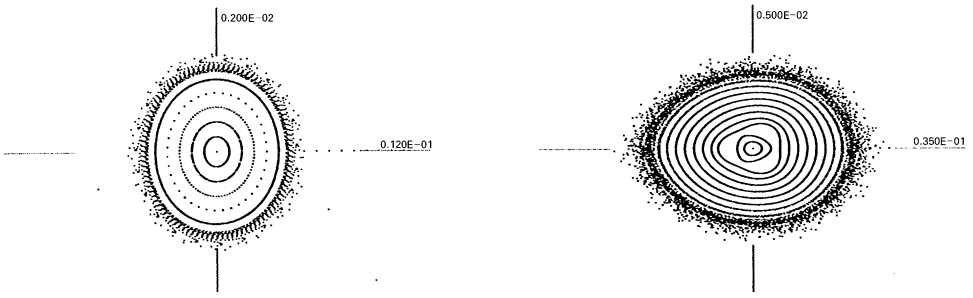

Fig. 2. Tracking pictures of on-energy particles launched along the x-axis with vanishing transversal momenta, magnet aperture of 75 mm, for two types of fringe fields.

Table 1
A few amplitude dependent tune shifts for the 75 mm aperture case. All 6 studied fringe field fall-off shapes are included

Type of fringe field	Amplitude dependent tune shifts				
	$(\nu_x\|J_x)$	$(\nu_x\|J_y)$	$(\nu_x\|J_x^2)$	$(\nu_x\|J_xJ_y)$	$(\nu_x\|J_y^2)$
Default dipole	957	1466	−16023679	456668857	−293452875
Default quadrupole	475	718	−416016	−1258842	−952296
Default sextupole	477	720	−239001	−721214	−544239
LHC HGQ lead end	1261	1773	−54679213	−227089388	−22890174
2 parameter Enge function	459	702	551115	12895677	−6894978
GSI QD	480	762	65222	36938218	4364284

the details of the fringe fields in particular. Hence, a careful study of fringe field effects appears to be indicated for detailed analysis of new lattices sensitive to nonlinearities, including the proposed Neutrino Factories and muon colliders. However, the design of these facilities is at an early stage, and no sufficiently detailed magnet designs are currently available. Thus, no realistic fringe field analysis is possible yet. On the other hand, complete magnet end designs are available for the Large Hadron Collider's interaction region High Gradient Quadrupoles. Thus, we consider various fringe field effects for the LHC and try to make inferences to the case of the Neutrino Factories.

During the last few years, many studies on single particle dynamics in the Large Hadron Collider to be built at CERN have been performed; for some of the results, see Ref. [5] and references therein,

and Ref. [6]. Specifically, at collision energy it has been shown that the dynamics is dominated by the interaction region's high gradient quadrupole triplets. This is mostly due to large variations of the β functions across the quadrupoles. The studies concentrated on many possible realizations of the LHC lattice, that is, on computing the effects of the so-called systematic and random body errors, and perhaps other effects like crossing angle, beam–beam interaction, misalignment, etc. The fringe fields, traditionally, are taken into account at most at the level of lumped thin lenses (kicks), characterized by integrated multipole strengths. However, it is not obvious whether this simplistic approach is enough to give an accurate account of the dynamics under the influence of fringe fields in all cases, and specifically for the muon machines in question.

The studies contained in the present paper are based on our results on Differential Algebraic field computation for realistic fields. In Refs. [7,8] it is shown how to take into account the local structure of s-dependent fields exactly based on a geometric representation of the coils as in the code ROXIE [9], resulting in the computation of very accurate fringe field maps. We use the fringe field maps computed with the methods of Ref. [7] to study systematically their effect on the nonlinear dynamics of the LHC. Their influence is measured by tuneshifts, resonance strengths and sometimes resonance webs. We also evaluate their relative importance with respect to body errors. Results concerning off-energy particles are also included.

2. Methods of analysis

As indicators, we use measures of the performance of existing accelerators, and which were useful for construction of correction schemes for proposed machines [10]. We will employ tune footprint, tune shift, and resonance web calculations. All of them are based on normal forms of symplectic maps. We assume that the machine of interest is accurately described by the nth order Taylor expansion $\mathcal{M}_n$ of the system's true map, $\mathcal{M}$. Because hadron accelerators can be regarded as large Hamiltonian systems, the truncated map will be symplectic to order n, satisfying $M^{\mathrm{T}}JM =_n J$. The truncated map can be subjected to an order by order symplectic change of variables that finally yields its normal form. That is, there exist symplectic maps $\mathcal{A}_n$ such that

$$\mathcal{N} = \mathcal{A}_n \circ \mathcal{M}_n \circ \mathcal{A}_n^{-1}. \tag{1}$$

The symplectic map $\mathcal{N}$ takes a particularly simple interpretation; it is a rotation with radius dependent frequency. See Refs. [10,11] for details. The angles of advancement of a point on a torus after one application of the map are called the tunes of the respective particle. Its deviation from the tune of a particle with zero amplitude (the linear tune) is called the tune shift. Due to the fact that the normal form of a symplectic map is unique, also the tune shifts are uniquely defined. We compute these quantities for the various cases studied. In general, for good performance of accelerators, large tune shifts are to be avoided.

In this setting, the resonance condition is defined as $\vec{k} \cdot \vec{\mu}(\vec{J}, \vec{\delta}) = m \,(\mathrm{mod}\, 2\pi)$, for a vector of integers $\vec{k}$ and integer m. The tunes are denoted by $\vec{\mu}$, and $\vec{J}$ represents the action variables (the radii), while $\vec{\delta}$ describes the parameters. Although the normal form transformation can be used to compute the tunes only in the non-resonant case, it is the expectation that extrapolation of the results close to the resonant case can give insight into the dynamics of resonant orbits. For this purpose, we study the above equation as a function of $\vec{J}$. By adding to the right-hand side a small quantity $\varepsilon \ll 1$ with fixed maximum value, we plot in action space the $\vec{J}$'s that satisfy the resonant condition. This gives direct insight into the resonant orbit structure of the phase space. This picture of the location and width of resonance lines is called the resonance web. The intuitive interpretation of the role of ε is that it translates a fixed small distance in tune space around exactly resonant orbits into oscillation of the action variables around exactly resonant orbits. The amount of oscillation gives a measure of the width of the resonance lines. Overlapping resonance lines are considered signs of chaos, which is not necessarily bad in theory, but in practice usually it is. Often, the dynamic aperture is close to the chaotic boundary. Hence,

the closeness of the resonance lines to the origin in action space again can be a useful indicator.

In passing we remind that none of the above indicators have an absolute correlation with the behavior of particles in accelerators. In some cases one of them can have a better correlation with the dynamic aperture, in other cases another indicator, or none. However, altogether probably they can reveal the gross features of the dynamics and are thus a useful analysis tool.

3. Cases studied

In order to assess fringe field effects, we will compare their contribution to that of the natural lattice. In addition, since the nonlinearities of the LHC are largely dominated by multipole errors, we will also compare the effects of the fringe fields to those of the multipole errors. Considering that the muon collider lattices have fewer elements, have larger deflections per magnet, a relatively larger aperture, and overall are more intrinsically nonlinear, it is expected that multipole errors will have a less drastic influence than in the case of the LHC; details have to wait until more specific information about magnet design are available.

All maps, for the fringe fields of the final focus quadrupoles and the rest of the lattice (LHC v.5.1), have been computed at order 8 using the code COSY Infinity [12]. Due to sensitivity to numerical errors, especially at high orders, of the tune-shift computation and occurrence of large numbers in the maps, we performed all the calculations in quadruple precision. The effects of RF cavities have been neglected, i.e., we computed the maps in two transversal degrees of freedom, with energy as a parameter. At the specific location of the lattice where we fixed the Poincare section, the r.m.s. beam sizes are $\sigma_x = 1.267 \times 10^{-4}$ m and $\sigma_y = 2.981 \times 10^{-4}$ m. It is also known from the design specifications that the r.m.s. normalized emittance is $\varepsilon_N = 3.75 \times 10^{-6}$ m r and the r.m.s. energy deviation is $\sigma_E = 1.1 \times 10^{-4}$.

For body errors, we used the Table MQXB (FNAL High Gradient Quad) Reference Harmonics at Collision v. 2.0 [13]. The detailed analysis of the body errors where not the main purpose of our studies, so we used only one seed for the random body errors, which gives "average" results in some sense (for example dynamic aperture), however, under the pessimistic assumption that the systematic part of the body errors assume the maximal value, with the two possible signs. That is, if we denote by $\langle b_n \rangle$ the average value of a multipole, then the multipole value due to uncertainty lies between $-d(b_n) + \langle b_n \rangle \leqslant b_n \leqslant + d(b_n) + \langle b_n \rangle$. Hereafter, we will refer to the two cases of full uncertainty by their sign, (−) or (+).

To assess the importance of fringe fields, for the High Gradient Quadrupoles we use the exact shape of the fringe field computed using the model HGQS01 [14], and for the rest of the elements a "default" fringe field shape. This generic fringe field is implemented in the code COSY Infinity, and it is based on the fall-off modeled by an Enge function [12]. The detailed fringe fields detune the ideal lattice and also introduce linear coupling between the planes. To allow meaningful comparisons of results, it is necessary to retune and decouple the lattice. We achieve this in a rather elegant way using an idealized local correction. Moreover, the method provides a way to keep the linear lattice design completely unchanged. It is done by splitting the fringe field maps in two parts $M_{ff} = L_{ff} + N_{ff}$, where L_{ff} is the linear part and N_{ff} is the nonlinear part. Application of the inverse of the linear map, which can be thought of as the zero length insertion ideal local corrector, we obtain for the fringe field map

$$\tilde{M}_{ff} = I + L_{ff}^{-1} \circ N_{ff} \tag{2}$$

where I is the identity map. The identity as linear part ensures that the linear layout of the lattice remains unchanged. Of course one would get a slightly different result if one were to apply L_{ff}^{-1} from the right. However, L_{ff} is close to identity, so L_{ff}^{-1} is also close to identity, and hence almost commutes with the nonlinear part. Again, this is an idealized case, and it is very likely that any real world correction scheme would introduce more nonlinearities in the map of the system. As a final remark, we mention that it is enough to compute only the exit focusing fringe field maps, and obtain the other variants by mirroring operations and rotations. Also, we use the same symmetry based

tricks to get the correct maps for the proposed layout of the interaction regions, which includes rotations of quadrupoles around their vertical axis. The respective procedures are described in Ref. [8].

Table 2 contains the cases studied. In the following section, we describe the results obtained for each of them. We will refer to the specific cases by their number in the table.

4. Results and discussion

The results shed light on the relative importance of intrinsic nonlinearities of the ideal lattice, the fringe field-induced nonlinearities, and body error-induced nonlinearities. The tunes are visualized in two different ways. The two-dimensional pictures represent the usual tune footprint style, and the three-dimensional pictures show the tune shift of particles as a function of initial amplitudes in geometric space, in units of r.m.s. beam sizes, up to 6σ. The tuneshifts in the three-dimensional pictures are all in units of 10^{-4}. The resonance strengths are computed close to the expected dynamic aperture, along the diagonal in action space. The units are arbitrary, and we denote $\vec{k} = (q, p)$. Every case is subdivided into three subcases according to energy: $\delta = -2.5\sigma_E, 0, +2.5\sigma_E$. For the computation of resonance webs, we used a maximum value of $\varepsilon = 10^{-3}$. The size of the beam at the expected dynamic aperture is approximately $J_x = J_y = 5 \times 10^{-4}$ m.

Table 2
The various cases studied

Case	System
1	Whole lattice at order 8 Fringe fields and body errors OFF
2	Whole lattice at order 8 Detailed fringe fields for HGQ, and default fringe fields for rest of ring ON; body errors OFF
3	Whole lattice at order 8 Fringe fields OFF, body errors (−) ON

We studied the nonlinearities of the ideal lattice, without any errors and only the intrinsic nonlinearities of the whole ring up to order 8. This is case 1, and the relevant figures are Figs. 3–5

We checked that the effects of the intrinsic nonlinearities of the whole lattice are comparable with those created by the fringe fields of the interaction regions. In fact, for the case $\delta < 0$ the fringe fields cause a bigger maximum tune shift, while for $\delta \geqslant 0$ the intrinsic nonlinearities are

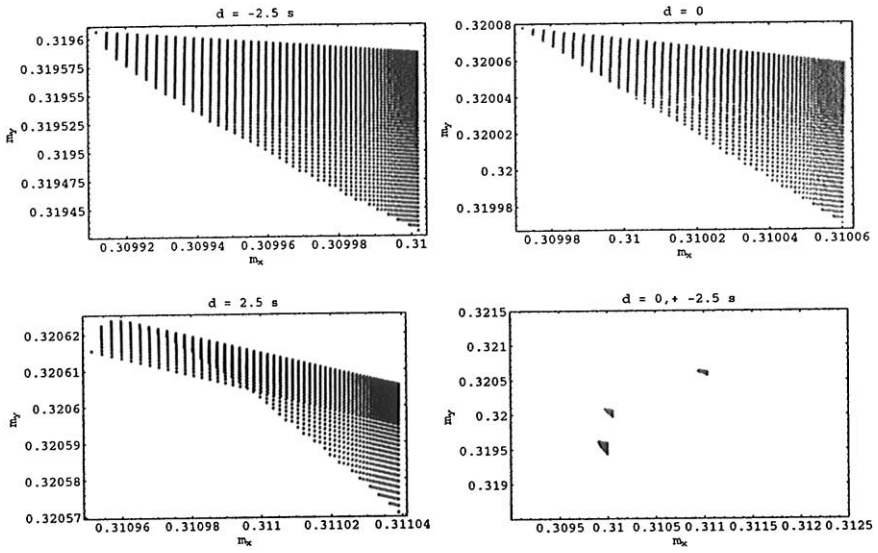

Fig. 3. Tune footprints for ideal lattice without fringe fields.

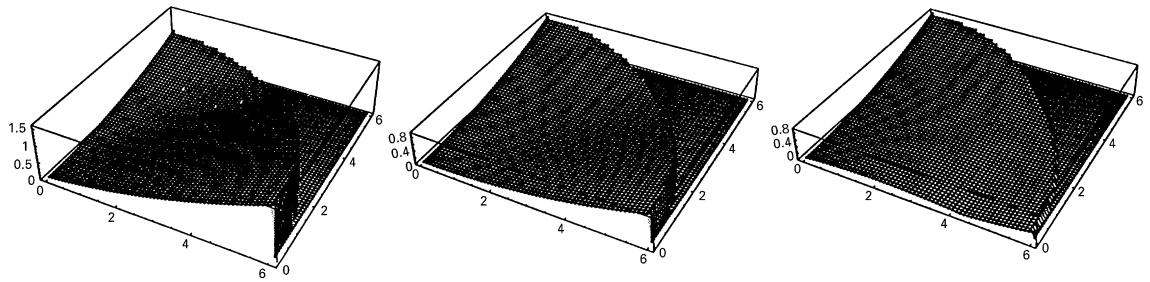

Fig. 4. Tune shifts for ideal lattice without fringe fields.

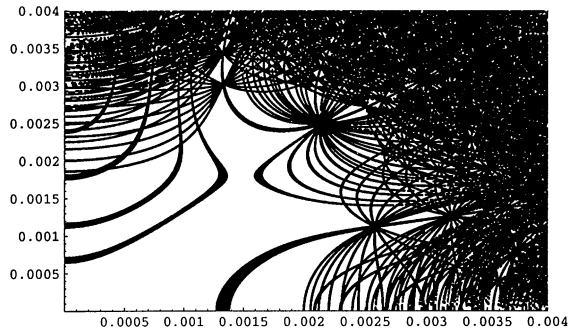

Fig. 5. Resonance web for ideal lattice without fringe fields, for $\delta = 0$.

marginally bigger. Also, the tune footprints are roughly the same, regular and triangle shaped. The resonance web shows the chaotic boundary to be at approximately 3×10^{-3} m. A beam of $\simeq 12\sigma_{x,y}$ occupies $\simeq 4 - 5 \times 10^{-4}$ m in this picture, therefore, this region is completely free of low order resonances. We estimated the following resonances to be the ''thickest'', in decreasing order: $(1, -1)$, $(2, -2)$, $(3, -3)$, $(4, -4)$, $(6, 1)$ and $(8, -1)$.

Case 2 represents the situation when fringe fields are set on for the whole ring. Figs. 6 and 7 show the tune shifts and footprints. We checked that the dominating fringe field effects are concentrated in the interaction regions, which has

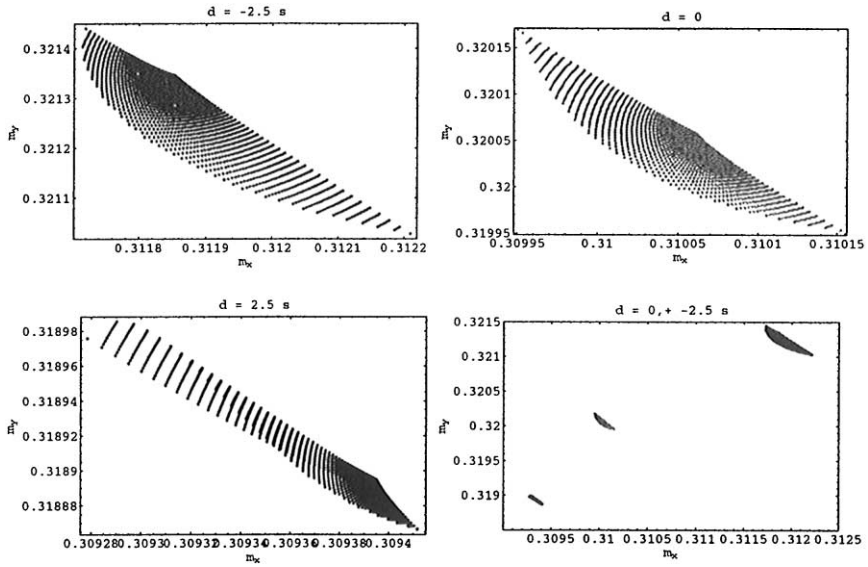

Fig. 6. Tune footprints for ideal lattice with fringe fields.

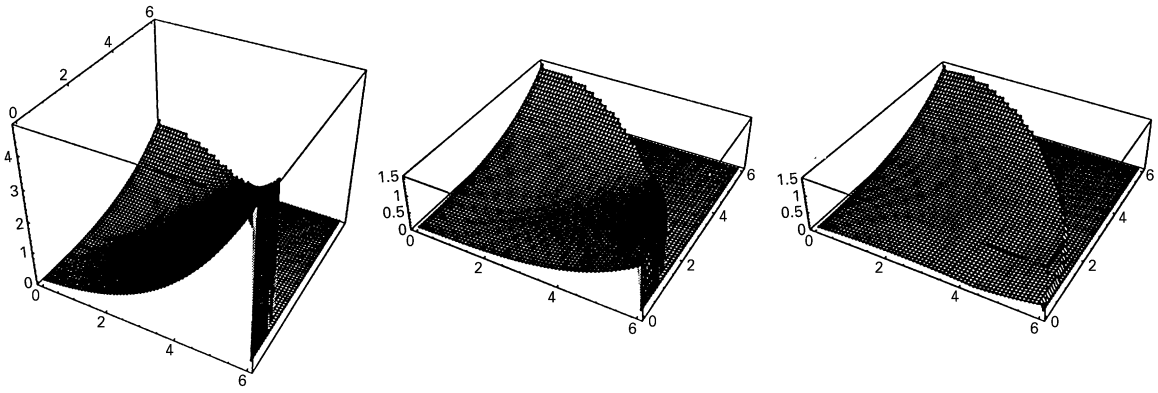

Fig. 7. Tune shifts for ideal lattice with fringe fields.

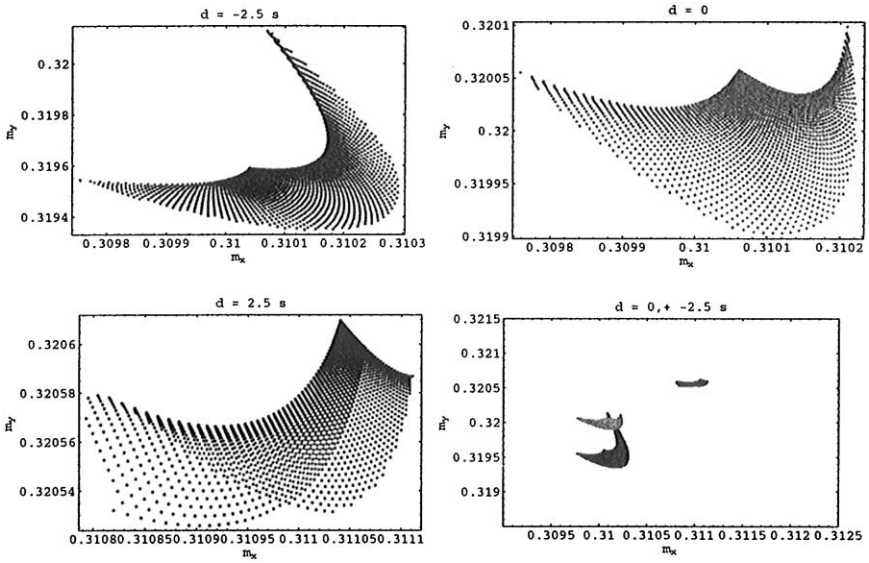

Fig. 8. Tune footprints for lattice with maximum body errors.

been showed to hold for other dynamic aperture limiting effects too.

The last case deals with the body errors. As mentioned in Section 3, we have two possible signs for the uncertainty part of the errors. We use the same "average" seed for the random part in both cases. As case 3, we employ the (−) case. For case 3, Figs. 8 and 9 show slightly bigger tune shifts and footprints than for case 2, but still inside the safe region. The footprints are elongated and curved, and even overlapping for $\delta = -2.5\sigma_E$ and $\delta = 0$, respectively.

5. Conclusions

In conclusion, the fringe fields generate important dynamical effects, visible in the tune shifts, footprints, and dynamic aperture. For the LHC, their magnitude is comparable to that of the nonlinearities generated by body errors, which here provide a larger contribution than in many other accelerators. In the worst case scenario, body errors induce nonlinearities that in the current model are roughly twice as large as those due to the fringe fields. Also the dynamic aperture

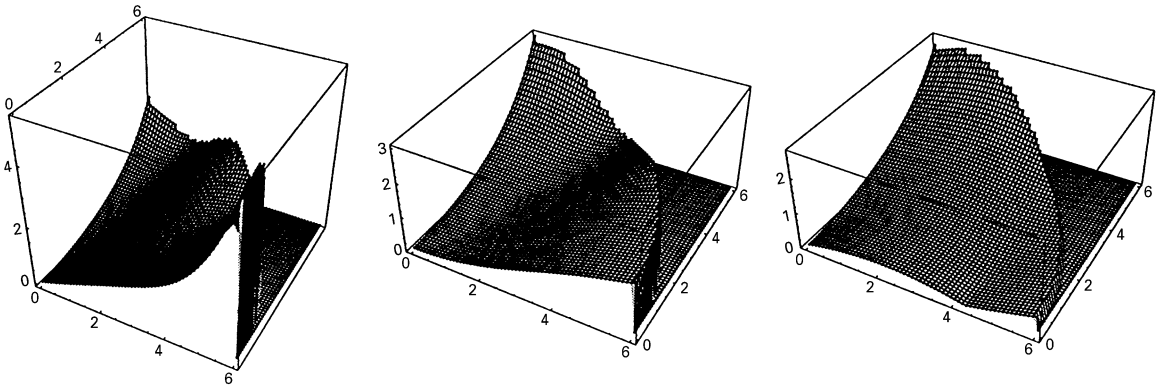

Fig. 9. Tune shifts for lattice with maximum body errors.

of the ideal lattice is drastically reduced solely due to fringe field effects, while still staying within an acceptable domain.

For the case of the Neutrino Factory, fringe fields generate effects that reduce the dynamic aperture by a similar factor compared to the natural ring. Extrapolating to the Neutrino Factory scenarios where body errors will likely not be as prominent as in the LHC, the fringe field effects may be expected to be an important contribution to the nonlinear effects, likely requiring adjustments in the linear design and nonlinear correction. Therefore, accurate fringe field maps are necessary for reliable simulations, and the design of appropriate magnet ends early in the design stage seems advisable.

References

[1] M. Berz, B. Erdelyi, K. Makino, Fringe field effects in small rings of large acceptance, Phys. Rev. ST-Accel. Beams 3 (2000) 124001.

[2] C. Johnstone, Collider ring lattices, Proceedings of HEMC'99, Workshop on Muon Colliders at Highest Energies, Long Island, Montauk, 1999.

[3] Y. Papaphilippou, D.T. Abell, Beam dynamics analysis and correction of magnet field imperfections in the SNS accumulator ring, Proceedings of the 2000 European Particle Accelerator Conference, Viena, JACoW, 2000.

[4] M. Berz, K. Makino, B. Erdelyi, Fringe field effects in Muon Rings, Proceedings of HEMC'99, Workshop on Muon Colliders at Highest Energies, Long Island, Montauk, 1999.

[5] J.-P. Koutchouk, The LHC dynamic aperture, Proceedings PAC'99, New York, AIP, 1999.

[6] B. Erdelyi, M. Berz, K. Makino, Detailed analysis of fringe field effects in the Large Hadron Collider, Technical Report MSUCL-1129, 1999.

[7] B. Erdelyi, M. Lindemann, M. Berz, Differential algebra based magnetic field computations and accurate fringe field maps, 2000, in preparation.

[8] B. Erdelyi, Ph.D. thesis, in preparation.

[9] S. Russenchuck, C. Paul, K. Preis, Roxie—a feature-based design and optimization program for superconducting accelerator magnets, Technical Report LHC Project Report 46, CERN, 1996.

[10] M. Berz, Applications of Modern Map Methods in Particle Beam Physics, Academic Press, Orlando, FL, ISBN 0-12-014750-5, 1999.

[11] M. Berz, Differential algebraic formulation of normal form theory, in: M. Berz, S. Martin, K. Ziegler (Eds.), Proceedings of the Nonlinear Effects in Accelerators, IOP Publishing, London, 1992, p. 77.

[12] K. Makino, M. Berz, Nucl. Instr. and Meth. A 427 (1999) 338.

[13] MQXB (FNAL High Gradient Quad) Reference Harmonics at Collision v.2.0, http://www.agsrhichome.bnl.gov/LHC/fnal/v2.0/hgq_col_v2p0.txt.

[14] G. Sabbi, Magnetic field analysis of HGQ coil ends, Technical Report TD-97-040, Fermilab, 1997.